

Carbon Nanostructures as an Electromechanical Bicontinuum

Cristiano Nisoli*, Paul E. Lammert*, Eric Mockensturm† and Vincent H. Crespi*

**Department of Physics and Materials Research Institute*

†*Department of Mechanical and Nuclear Engineering*

The Pennsylvania State University, University Park, PA 16802-6300

(Dated: November 2, 2018)

A two-field model provides an unifying framework for elasticity, lattice dynamics and electromechanical coupling in graphene and carbon nanotubes, describes optical phonons, nontrivial acoustic branches, strain-induced gap opening, gap-induced phonon softening, doping-induced deformations, and even the hexagonal graphenic Brillouin zone, and thus explains and extends a previously disparate accumulation of analytical and computational results.

PACS numbers: 62.25.+g, 81.05.Tp, 63.22.+m, 77.65.-j, 46.05.+b

Vibrations in carbon nanostructures such as tubes, fullerenes, or graphene sheets [1, 2, 3] have a ubiquitous influence on electronic, optical and thermal response: scattering from optical phonons limits charge transport in otherwise ballistic nanotube conductors [4, 5]; twist deformations gap metallic tubes [6, 7]; ballistic phonons transport heat in nanotubes with great efficiency [8, 9, 10]; resonant Raman spectroscopy can unambiguously identify a tube's wrapping indices (n,m) [11, 12, 13, 14]; electron-phonon interactions may ultimately limit the electrical performance of graphene [15, 16]. Computationally intensive atomistic models of lattice dynamics often lack simplified model descriptions that can facilitate insight, yet traditional analytical continuum models [1, 2, 17, 18], while very useful and important, cannot describe atomistic phenomena without phenomenological extensions [19, 20, 21]. Although continuum models are restricted to long-wavelength physics, they have been used to describe atomic-scale phenomena in bulk binary compounds by incorporating a separate continuum field for each sublattice [23]: in graphene, two fields are necessary. Here we present an analytical “bicontinuum” model that represents the full atomistic detail of the graphenic lattice, including optical modes, nonlinear dispersion of in-plane phonons, electromechanical effects and even the hexagonal graphenic Brillouin zone, a construct generally held to be exclusively atomistic.

Graphene decomposes into the two triangular sublattices of Fig. 1. We describe in-plane deformations of the sublattices via two fields, $u^i(x)$, $v^i(x)$, $i = 1, 2$, and their strain tensors $u^{ij} = \partial^{(i}u^{j)}$ and $v^{ij} = \partial^{(j}v^{i)}$. The density of elastic energy contains direct and cross terms:

$$V[u, v] = d[u] + d[v] + c[u, v]. \quad (1)$$

Six-fold symmetry of the sublattices implies isotropy of the direct terms [24]:

$$d[u] = \mu' u^{ij}u_{ij} + \frac{\lambda'}{2} u_i^i u_j^j. \quad (2)$$

Symmetry dictates the form of the cross term

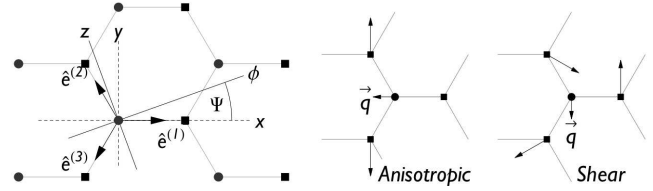


FIG. 1: The two sublattices (circles and squares) of graphene and the three unit vectors $\hat{e}^{(l)}$ used in the text. ϕ , z are cylindrical coordinates of a tube, while $\Psi = \pi/6 - \theta_c$ with θ_c the chiral angle. Also, anisotropic ($u^{xx} = u^{xy} = 0$, $u^{yy} = 2\gamma$, $q^x = \ell\gamma$), shear ($u^{xx} = u^{yy} = 0$, $u^{xy} = \eta$, $q^y = -\ell\eta$) strains.

$$c[u, v] = 2\mu u^{ij}v_{ij} + \lambda u_i^i v_j^j + \alpha(u - v)^2 - \beta e_{ijk}(u^{ij} + v^{ij})(u^k - v^k) \quad (3)$$

The tensor e_{ijk} , which is invariant under C_{3v} , can be represented by the three unit vectors $\{\hat{e}^{(l)}\}$ of Fig. 1:

$$e_{ijk} = \frac{4}{3} \sum_{l=1}^3 \hat{e}_i^{(l)} \hat{e}_j^{(l)} \hat{e}_k^{(l)}. \quad (4)$$

Only the last term in Eq. 4 is not invariant under general rotation. (In nanotubes, it depends on the helical angle θ_c : $e_{\phi\phi\phi} = -e_{\phi zz} = -\sin(3\theta_c)$, $e_{zzz} = -e_{\phi\phi z} = -\cos(3\theta_c)$, where ϕ , z are defined in Fig. 1). This elastic energy density, the lowest-order approximation in both derivatives and fields, contains six parameters: μ' and λ' , being confined to one sublattice, describe next-neighbor interactions; the cross terms μ and λ describe nearest-neighbor interaction; α describes the stiffness against relative shifts of the sublattices; β determines the strength of rotational symmetry breaking and so carries the point group symmetry of graphene. These parameters are normalized to the sublattice surface density σ_s , so that the elastic energy is $W = \int \sigma_s V d^2x$.

Taking $\frac{1}{2}\sigma_s(\dot{u}^2 + \dot{v}^2)$ as the surface density of kinetic

energy, the equations of motion read

$$\begin{cases} \ddot{u}^i = \partial_j \sigma_{(u)}^{ij} - 2\alpha (u^i - v^i) + \beta e_{lm}^i (v^{lm} + u^{lm}) \\ \ddot{v}^i = \partial_j \sigma_{(v)}^{ij} + 2\alpha (u^i - v^i) - \beta e_{lm}^i (v^{lm} + u^{lm}) \end{cases} \quad (5)$$

with the sublattice 2-D stress tensors

$$\begin{cases} \sigma_{(u)}^{ij} = 2\mu' u^{ij} + \lambda' \delta^{ij} u_k^k + 2\mu v^{ij} + \lambda \delta^{ij} v_k^k \\ \quad - \beta e_{ij}^k (u^k - v^k) \\ \sigma_{(v)}^{ij} = 2\mu' v^{ij} + \lambda' \delta^{ij} v_k^k + 2\mu u^{ij} + \lambda \delta^{ij} u_k^k \\ \quad - \beta e_{ij}^k (u^k - v^k) \end{cases} \quad (6)$$

As expected, α determines the frequency of two degenerate $k = 0$ optical modes: $\omega_{\Gamma^2} = 4\alpha$.

First, we briefly show that the usual macroscopic elastic energy of graphene and its Lamé coefficients can be obtained from V by considering a static, uniform solution of Eqs. 5 with identical deformations on both lattices with an internal displacement $2q^i \equiv u^i - v^i$:

$$2q^i = \ell e_{lm}^i u^{lm} = \ell e_{lm}^i v^{lm}, \quad (7)$$

where $\ell = \beta/\alpha$ is a characteristic length. Anisotropic ($2\gamma = u^{xx} - u^{yy}$) and shear ($\eta = u^{xy}$) strains produce internal displacements $q^x = \ell\gamma$ and $q^y = -\ell\eta$ (Fig. 1). The elastic energy for uniform deformations $W_u = \int V_u \sigma_g d^2x$ then simplifies to

$$\begin{aligned} V_u[u, q] = & \left(\mu_R + \frac{\beta^2}{\alpha} \right) u^{ij} u_{ij} + \frac{1}{2} \left(\lambda_R - \frac{\beta^2}{\alpha} \right) u_i^i u_j^j \\ & + 2\alpha q^2 - 2\beta e_{ijk} u^{ij} q^k, \end{aligned} \quad (8)$$

where $\sigma_g = 2\sigma_s = 2.26 \text{ g cm}^{-2}$ is the surface density of graphene, $\mu_R \equiv \mu + \mu' - \frac{\beta^2}{\alpha}$, $\lambda_R \equiv \lambda + \lambda' + \frac{\beta^2}{\alpha}$ the measurable Lamé coefficients [24]. Macroscopic problems do not distinguish between the two sublattices; eliminating q^i in Eq. 8 through Eqs. 4 and 7 we obtain the familiar, isotropic, macroscopic energy for graphene, $V_u = \mu_R u^{ij} u_{ij} + \lambda_R u_i^i u_j^j / 2$. In the long wavelength limit Eqs. 5 returns the familiar longitudinal and transverse speeds of sound in terms of the Lamé coefficients: $v_L^2 = 2\mu_R + \lambda_R$, $v_T^2 = \mu_R$.

The out-of-plane displacements $u_{\perp}(x)$ and $v_{\perp}(x)$ do not couple with the in-plane u^i, v^i in the harmonic limit: invariance under simultaneous sign change of u_{\perp} and v_{\perp} prevents it, for flat sheets. Introducing $2p_{\perp}(x) = u_{\perp}(x) + v_{\perp}(x)$ and $2q_{\perp}(x) = u_{\perp}(x) - v_{\perp}(x)$, V_{\perp} must be invariant under $p_{\perp} \rightarrow p_{\perp} + L(x)$, $L(x)$ a linear function in the plane, and thus, can contain only second (and higher) derivatives in p_{\perp} . Symmetry dictates (cf. Appendix)

$$\begin{aligned} V_{\perp} = & 4\alpha_{\perp} q_{\perp}^2 - 4\alpha'_{\perp} \partial_i q_{\perp} \partial^i q_{\perp} + 4\beta_{\perp} e_{ijk} \partial^k q_{\perp} \partial^{ij} p_{\perp} \\ & + 2\mu_{\perp}^+ \partial_{ij} p_{\perp} \partial^{ij} p_{\perp} + \lambda_{\perp}^+ \partial_i^i p_{\perp} \partial_i^i p_{\perp} \\ & - 2\mu_{\perp}^- \partial_{ij} q_{\perp} \partial^{ij} q_{\perp} - \lambda_{\perp}^- \partial_i^i q_{\perp} \partial_i^i q_{\perp}. \end{aligned} \quad (9)$$

The frequency of the $k = 0$ out-of-plane optical mode is $2\sqrt{\alpha_{\perp}}$, and the out-of-plane acoustic branch is quadratic at small wave-vector, as expected.

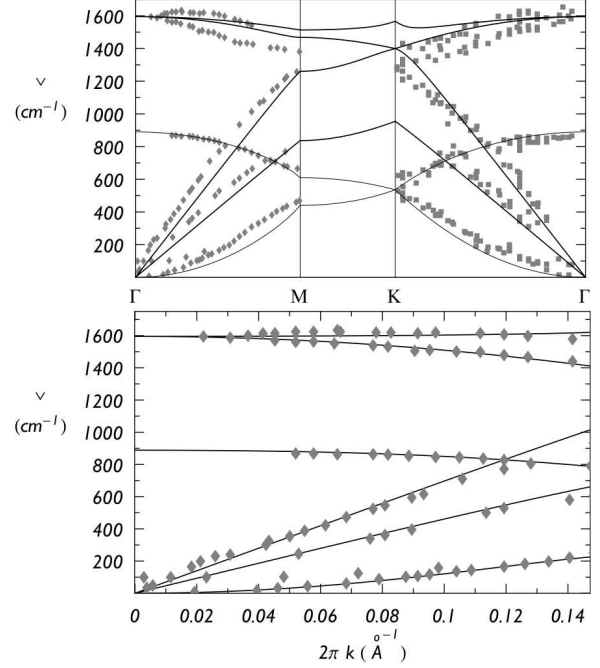


FIG. 2: Bicontinuum phonons compared to EELS data (diamonds [26] and squares [27]), fitting either to the entire Brillouin zone (top) or just around Γ along $\Gamma \rightarrow M$.

The bicontinuum phonons are much more richly structured than in a traditional continuum model: they include all the optical branches, show nonlinear dispersion at large wavevector, and even display the main features of the Brillouin zone, all without sacrificing the advantages of a continuum framework. Plane-wave solutions of Eqs. 5 returns an analytically solvable fourth-order secular equation in $\omega(k)$, yielding two acoustic and two optical branches. The longitudinal branches cross at the vertices of a hexagon. Since the two-field elastic energy density respects the point group symmetry of the graphene lattice, this hexagon is oriented just as the graphene Brillouin zone; although the model, unlike in the envelope function approach [25], has no built-in length scale, the elastic parameters can be constrained so that the crossing point coincides with the K point of graphene. A similar argument holds for the out-of-plane modes: strikingly *one can construct the correct Brillouin zone within a continuum model*. Fig. 2 shows the bicontinuum phonons fit to electron-energy-loss spectroscopy (EELS) data [26, 27] for parameters fitted either to the full Brillouin zone or just around Γ [28].

The bicontinuum provides a unified framework for nanotube mechanics which can describe *all* current computational results on the coupling of nanotube phonons to static structural distortions, to each other (e.g. breathing-to-Raman or longitudinal-to-transverse modes in helical tubes) and to the tube electronic structure. In a cylindrical geometry with coordinates $\{r, \phi, z\}$, a

coupling between the tangential displacements u^i , and the radial $u^r = u_\perp$ appears in V of Eq. 1 via $u^{\phi\phi} = (\partial_\phi u^\phi + u^r)/r$ (and similarly for v); this accounts for the emergence of the Radial Breathing Mode (RBM) [29]. We consider uniform solutions: $u = u_o e^{-i\omega t}$, $v = v_o e^{-i\omega t}$. The tube's helicity can be subsumed into new axes $\{\xi, \zeta\}$ ($\xi = \phi \cos 3\theta_c + z \sin 3\theta_c$, $\zeta = -\phi \sin 3\theta_c + z \cos 3\theta_c$) rotated by an angle $3\theta_c$ with respect to the base of the tube. In terms of p, q we obtain $p^\xi, p^\zeta = 0$ and

$$\begin{cases} q^\zeta (\omega^2 - 4\alpha) + 2\frac{\beta}{r} p^r = 0 \\ p^r \left(\omega^2 - \frac{v_L^2 + \beta^2/\alpha}{r^2} \right) + 2\frac{\beta}{r} q^\zeta = 0 \\ q^\xi (\omega^2 - 4\alpha) = 0 \\ q^r \left(\omega^2 - 4\alpha_\perp + \frac{2\mu - 2\mu' + \lambda - \lambda'}{r^2} \right) = 0 \end{cases} \quad (10)$$

Unlike standard elasticity [17], which cannot describe optical modes, or standard atomistic descriptions, which cannot be solved analytically, the two-field continuum model enables an exact analytical solution for the coupling between the RBM and the graphite-like optical mode through the first two of Eqs. in (10); the RBM induces a shear in the sublattices, $u^{\phi\phi} = v^{\phi\phi} = u^r/r$, which couples with the internal displacement through β , and vice versa. Thus, the RBM is not purely radial, but has a longitudinal component $q_B^z \sim \frac{\ell}{2r} \cos 3\theta_c$, as previously seen in a numerical calculation [30]. Expansion of the RBM frequency in powers of l/r reveals a correction to the standard continuum result v_L/r [17]: $\omega_B = \frac{v_L}{r} \left[1 - \frac{1}{8} \left(\frac{\ell}{r} \right)^2 + O \left(\frac{\ell}{r} \right)^4 \right]$. The graphite-like optical modes of chiral tubes are $\omega_\xi = \sqrt{4\alpha}$, $\omega_\zeta/\omega_\xi = 1 + \frac{1}{8} \left(\frac{\ell}{r} \right)^2 + O \left(\frac{\ell}{r} \right)^4$, also of mixed longitudinal/transverse character except for armchair and zig-zag nanotubes, while the out-of-plane optical mode $\omega_\perp = \left(4\alpha_\perp - \frac{2\mu - 2\mu' + \lambda - \lambda'}{r^2} \right)^{1/2}$ is purely radial. A density functional theory calculation of the breathing mode [31] reports different frequencies with (ω_B) and without $(\tilde{\omega}_B)$ coupling to optical modes. We predict $r^2 (\tilde{\omega}_B^2 - \omega_B^2) \rightarrow \beta^2/\alpha$ as $r \rightarrow \infty$: using ref [31] data for $\tilde{\omega}_B, \omega_B$ we obtain $\ell \equiv \beta/\alpha = 0.25 \text{ \AA}$ (0.27 \AA) for non metallic zig-zag (armchair) tubes, in good agreement with the parameters from our fit to the graphene phonons [28].

The bicontinuum can also describe electron-lattice coupling to both acoustic and optical modes, by incorporating a tight-binding model whose nearest neighbor hopping integrals $t^{(1)}, t^{(2)}, t^{(3)}$ are modulated by the in-plane elastic deformations:

$$dt^{(l)} = -\tau \hat{e}_i^{(l)} \hat{e}_j^{(l)} u^{ij} + \tau \hat{e}_i^{(l)} q^i/e \quad (11)$$

where e is the inter-atomic distance and τ a parameter to be determined [32]. For example, lattice deformations open gaps in metallic tubes, and these gaps in turn affect vibrational frequencies. If ϵ_c, ϵ_v are the conduction and

valence bands, we have to nearest neighbors

$$\epsilon_c(k)^2 - \epsilon_v(k)^2 = \sum_l t^{(l)} + 2 \sum_{m>l} t^{(l)} t^{(m)} \cos(k \cdot a^{(n)}), \quad (12)$$

where $a^{(n)} \equiv e^{(l)} - e^{(m)}$, $n(l, m)$ is cyclic in $\{1, 2, 3\}$ (e.g. $a^{(3)} \equiv e^{(1)} - e^{(2)}$) and $\{e^{(i)}\}$ connects nearest neighbors. From Eqs. 11,12 we find the band gap opened by strain in a metallic nanotube to be

$$\begin{aligned} \frac{\Delta^2}{(3\tau)^2} &= \frac{1}{2} u^{ij} u_{ij} - \frac{1}{4} u_i^i u_i^i - \frac{1}{e} e_{ijk} u^{ij} q^k \\ &+ \frac{1}{e^2} (\hat{z}_i q^i)^2 + \frac{1}{e} e_{ijk} \hat{\phi}^k u^{ij} \hat{\phi}_h q^h - \frac{1}{4} (e_{ijk} u^{ij} \hat{\phi}^k)^2. \end{aligned} \quad (13)$$

In the second line of equation (13) the symmetry of the honeycomb lattice is broken by the unit vectors $\hat{\phi}^i, \hat{z}^i$ of the cylindrical coordinates. In terms of $2\gamma' \equiv u^{\phi\phi} - u^{zz}$, $\eta' \equiv u^{\phi z}, q^z$, equation (13) reads

$$\Delta = 3\tau |q^z/e + \gamma' \cos(3\theta_c) + \eta' \sin(3\theta_c)|, \quad (14)$$

which corrects and extends a well known previous result within a one-field continuum model [7] that neglected the inner displacement (i.e. $q^i = 0$).

Opening bandgaps in metallic nanotubes causes several shifts in observed quantities. The term proportional to q_z^2 in Eq. (13) show that longitudinal optical modes open a bandgap in metallic tubes of any helicity; the elastic energy lowers by a term proportional to the square of the bandgap, leading to a the softening of longitudinal optical frequency in metallic nanotubes, as revealed by a recent DFT study [33]. Eq. (13) predicts also a softening of the RBM in metallic nanotubes $\frac{\delta\omega_B}{\omega_B} = -A \cos^2(3\theta_c)$, highest for zig-zag tubes as seen in DFT [31], and relates it to the optical softening, with $A = (1 - \ell/e)\omega_{opt}\delta\omega_{opt}e^2/4v_L^2$, ω_{opt} the graphite-like optical mode, and $\delta\omega_{opt}$ its softening in metallic tubes ($A \simeq 2\%$). Other shifts can be predicted: the speed of sound for the twist mode softens by $\frac{\Delta c_t}{c_t} = -\frac{v_L^2}{2v_T^2} A \sin^2(3\theta_c)$, or $\simeq 2.2\%$ in armchair tubes.

Doping-induced structural deformations can also be studied by minimizing the total energy (elastic plus doped electrons). Subtle phenomena absent in other models [22] can be accessed within the bicontinuum framework. Going to next-nearest-neighbor in the hopping integrals ($dt_1^{(l)} = -\tau_1 \hat{a}_i^{(l)} \hat{a}_j^{(l)} v^{ij}$ [32]), we find that at first order in both a/r and the number of dopant electrons per atom ρ_e , semiconducting $(n, 0)$ nanotubes show doping-induced changes in tube length ($dL/L = u^{zz}$) and axial bond-length ($db_{ax} = eu^{zz} - q^z$):

$$\begin{cases} dL/L = \frac{\rho_e \tau}{8m_C v_T^2} \left[\pm \left(1 - \frac{\ell}{e} \right) + \frac{3\tau_1}{2\tau} \frac{2\mu_R + \lambda_R}{\mu_R + \lambda_R} \right] \\ db_{ax} = \pm \frac{\rho_e \tau}{2m_C \omega_{opt}^2 e} \end{cases} \quad (15)$$

where m_C is the mass of the carbon atom. The sign is positive (negative) for $r = n \pmod 3 = 2$ ($n \pmod 3 = 1$).

Recent DFT results [34] indeed show shrinking or stretching of b_{ax} for $n = 16, 13$ or $n = 14, 11$ tubes respectively, as predicted by Eq. 15. In DFT, the overall tube lengthens in the second case ($n = 14, 11$), again in accord with the bicontinuum; the lengthening found for $r = 2$, is less than for $r = 1$, perhaps a consequence of the change in sign in Eqs. 15. Finally the shrinking of the axial bond determines an up-shift in the longitudinal graphite-like optical mode and might explain recent Raman results that point toward anomalous bond contraction under doping in semiconducting nanotubes [35, 36].

In summary, a symmetrized two-field continuum model of graphene and carbon nanotubes provides the first unified analytical treatment for a wide range of vibrational and electromechanical phenomena including nonlinear dispersion of in-plane phonons, zone-edge degeneracies and optical modes. A full range of vibrational-electronic-mechanical couplings, which were absent from previous continuum models or happened upon in an ad hoc fashion in computational work, can now be understood within a single unified analytical framework. Extending the formalism to include higher-order effects arising from curvature or metallic character (i.e. symmetry breaking terms containing $\hat{\phi}^i$, \hat{z}^i , as in Eq. 13), anharmonicity (terms higher order in u^{ij} , v^{ij}), or long-distance interactions (higher partial derivatives) is straightforward. An extension to boron nitride nanotubes, with different coefficients for each sublattice in the direct terms of Eq. 2, might prove useful to study their piezoelectricity.

Appendix: Derivation of Eq. 3

The term $c[u, v]$ must be invariant under the combination of $2\pi/6$ rotations and the exchange of fields $u \leftrightarrow v$. Adding reflection through the x axis (Fig. 1) then implies C_{3v} invariance. There is also a field translation invariance: $u(x) \rightarrow u(x) + p$, $v(x) \rightarrow v(x) + p$. The objects u^i , v^j , u^{ij} , and v^{ij} can be combined pairwise only into tensors of rank two, three and four; thus $c[u, v]$ decomposes into three parts. The first part has terms like $u^i v^j$; symmetry then implies the form $\alpha(u - v)^2$ with $\alpha > 0$ to ensure an energy minimum. The second part has terms like $u^{ij} v^{kl}$; the only admissible form is $2\mu u^{ij} v_{ij} + \lambda u_i^i v_j^j$. The third part contains only rank three terms such as $u^{ij} v^k$ contracted with a C_{3v} invariant tensor e_{ijk} , giving $e_{ijk} u^{ij} v^k$. By requiring invariance under $2\pi/6$ rotations conjugated with sublattice switching, and also the field translation invariance, we obtain the form $e_{ijk} u^{ij} (u^k - v^k) + e_{ijk}^* v^{ij} (v^k - u^k)$, where the star means a $2\pi/6$ rotation. Since C_{3v} invariance implies $e_{ijk}^* = -e_{ijk}$ we finally obtain the third row of Eq. 3.

[1] S. Iijima, Nature (London) **354**, 56 (1991).

[2] R. Saito, G. Dresselhaus and M. S. Dresselhaus, *Physical properties of Carbon Nanotubes* (Imperial College Press, London 1998).

- [3] M. S. Dresselhaus, G. Dresselhaus and P. C. Eklund, *Science of Fullerenes and Carbon Nanotubes* (Academic, New York, 1996).
- [4] S. J. Tans et al., Nature **386**, 474 (1997).
- [5] C. L. Kane et al., Europhys. Lett. **41**, 683 (1998).
- [6] A. Rochefort, P. Avouris, F. Lesage, D. R. Salahub, Phys. Rev. B **60**, 13824 (1999).
- [7] L. Yang and J. Han, Phys. Rev. Lett. **85**, 154 (2000)
- [8] S. Berber, Y-K. Kwon, and D. Tománek, Phys. Rev. Lett. **84**, 4613 (2000).
- [9] H.-Y. Chiu et al., Phys. Rev. Lett. **95**, 226101 (2005).
- [10] P. Kim, L. Shi, A. Majumdar and P. L. McEuen Phys. Rev. Lett. **87**, 215502 (2001).
- [11] E. Richter and K. R. Subbaswamy Phys. Rev. Lett. **79**, 2738 (1997).
- [12] R. Saito et al., Phys. Rev. B **64**, 085312 (2001).
- [13] A. Jorio et al., Phys. Rev. Lett. **86**, 1118 (2001).
- [14] A. Jorio, R. Saito, G. Dresselhaus and M. S. Dresselhaus, Phil. Trans. R. Soc. Lond. A **362**, 2311 (2004).
- [15] K. S. Novoselov et al., Nature **438**, 197 (2005).
- [16] S. Y. Zhou et al., Nature Phys. **2**, 595 (2006).
- [17] G. D. Mahan, Phys. Rev. B **65**, 235402 (2002).
- [18] H. Suzuura and T. Ando, Phys. Rev. B **65**, 235412 (2002); A. Raichura et al., J. Appl. Phys. **94**, 4060 (2003). S.V. Goupalov, Phys. Rev. B **71**, 085420 (2005)
- [19] F. Comas et al., Phys. Rev. B **47**, 7602 (1993).
- [20] L. Chico and R. Pérez-Álvarez Phys. Rev. B **69**, 35419 (2004). L. Chico and R. Pérez-Álvarez, Phys. Rev. B **73**, 075425 (2006)
- [21] Y. N. Gartstein et al., Phys. Rev. B **68**, 115415 (2003)
- [22] M. Verissimo-Alves, B. Koiller, H. Chacham, and R. B. Capaz, Phys. Rev. B **67**, 161401 (R) (2003).
- [23] H. Deresiewicz et al. *The collected papers of Raymond D. Mindlin*, Springer-Verlag New York (1989).
- [24] L. D. Landau, E. M. Lifshitz "Theory of Elasticity" Pergamon Press Oxford (1986). The density of elastic energy for an isotropic system has the form $f = \mu u^{ij} u_{ij} + \frac{\lambda}{2} u_i^i u_j^j$, where λ , μ are the Lamé coefficients. Here we renormalize the coefficients to $\sigma_g = 1$.
- [25] B. A. Foreman, Phys. Rev. B **52**, 12260 (1995).
- [26] C. Oshima et al., Solid State Commun. **65**, 1601 (1988).
- [27] S. Siebentritt, R. Pues, K. H. Rieder, and A. M. Shikin, Phys. Rev. B **55**, 7927 (1997).
- [28] The fit around Γ returns (in Km s^{-1}) $v_L = 21$, $v_T = 14$, $(-2\mu + 2\mu' - \lambda + \lambda' + \beta^2/\alpha)^{1/2} = 4.4$, $(\mu - \mu')^{1/2} = 15, 6$ and $\ell \equiv \beta/\alpha = 0.3 \text{ \AA}$ [28]. The fit to the full zone uses $v_L = 16.5 \text{ Km s}^{-1}$, $v_T = 10.8 \text{ Km s}^{-1}$, $(2\mu - 2\mu' + \lambda - \lambda' - \beta^2/\alpha)^{1/2} = 8.7 \text{ Km s}^{-1}$, $(\mu - \mu')^{1/2} = 6, 6 \text{ Km s}^{-1}$, $\ell \equiv \beta/\alpha = 0.24 \text{ \AA}$; an extension to higher derivatives would improve the agreement.
- [29] The chiral vector of the tube breaks the hexagonal symmetry and allows for new terms to be introduced in V as curvature corrections, which for simplicity we won't consider here. Different problems will suggest different leading corrections.
- [30] E. Dobardžić et al., Phys. Rev. B **68**, 045408 (2003).
- [31] J. Kürti et al., New J. Phys. **5**, 125 (2003).
- [32] $t^{(l)}$, $t_1^{(l)}$ are the absolute values of the hopping integrals for nearest and next nearest neighbors. We assume they depend only on distance, and thus $dt = -\tau de/e$, $dt_1 = -\tau_1 da/a$.
- [33] O. Dubay et al., Phys. Rev. Lett. **88**, 235506 (2002).

- [34] R. E. Margine *et al.* submitted to Phys. Rev. Lett.
- [35] G. Chen, C. A. Furtado, U. J. Kim, and P. C. Eklund
Phys. Rev. B **72** 155406 (2005).
- [36] G. Chen, C. A. Furtado, S. Bandow, S. Iijima and
P. C. Eklund Phys. Rev. B **71** 045408 (2005).